Quantum metasurface for multi-photon interference and state reconstruction

Kai Wang,[1,*] James G. Titchener,[1,2] Sergey S. Kruk,[1] Lei Xu,[1] Hung-Pin Chung,[1,3] Matthew Parry,[1] Ivan I. Kravchenko,[4] Yen-Hung Chen,[3,5] Alexander S. Solntsev,[1,6] Yuri S. Kivshar,[1] Dragomir N. Neshev,[1] Andrey A. Sukhorukov[1]

[1]Nonlinear Physics Centre, Research School of Physics and Engineering,
The Australian National University, Canberra, ACT 2601, Australia
[2]Quantum Technology Enterprise Centre, Quantum Engineering Technology Labs,
H. H. Wills Physics Laboratory and Department of Electrical and Electronic Engineering,
University of Bristol, BS8 1FD, UK
[3]Department of Optics and Photonics, National Central University, Jhongli 320, Taiwan
[4]Center for Nanophase Materials Sciences, Oak Ridge National Laboratory,
Oak Ridge, Tennessee 37831, USA
[5]Center for Astronautical Physics and Engineering, National Central University, Jhongli 320, Taiwan
[6]School of Mathematical and Physical Sciences, University of Technology Sydney,
Ultimo, NSW 2007, Australia

[*]To whom correspondence should be addressed; E-mail: kai.wang@anu.edu.au.

Metasurfaces based on resonant nanophotonic structures have enabled novel types of flat-optics devices often outperforming the capabilities of bulk components, yet these advances remain largely unexplored for quantum applications. We show that non-classical multi-photon interferences can be achieved at the subwavelength scale in all-dielectric metasurfaces. We simultaneously image multiple projections of quantum states with a single metasurface, enabling a robust reconstruction of amplitude, phase, coherence, and entangle-

1

ment of multi-photon polarization-encoded states. One- and two-photon states are reconstructed through nonlocal photon correlation measurements with polarization-insensitive click-detectors positioned after the metasurface, and the scalability to higher photon numbers is established theoretically. Our work illustrates the feasibility of ultra-thin quantum metadevices for the manipulation and measurement of multi-photon quantum states with applications in free-space quantum imaging and communications.

The field of nanostructured metasurfaces offers the possibility of replacing traditionally bulky imaging systems with flat optics devices (*1*) achieving high transmission based on all-dielectric platforms (*2–7*). The metasurfaces provide a freedom to tailor the light interference by coherently selecting and mixing different components on a sub-wavelength scale, enabling polarization-spatial conversion (*4*, *7–12*) and spin-orbital transformation (*13*). Such capabilities motivated multiple applications for the regime of classical light, yet the metasurfaces have a potential to emerge as essential components for quantum photonics (*14–17*).

The key manifestations of quantum light are associated with non-classical multi-photon interference, which is an enabling phenomenon for the transformation and measurement of quantum states. Conventionally, manipulation of multi-photon states is performed through a sequence of beam-splitting optical elements, each realizing quantum interference (*18–20*). Recent advances in nanotechnology enabled the integration of beam-splitters and couplers on tailored plasmonic structures (*21*, *22*), yet material losses and complex photon-plasmon coupling interfaces restrict the platform scalability. We realize several multi-photon interferences in a single flat all-dielectric metasurface. The parallel quantum state transformations are encoded in multiple interleaved metagratings, taking advantage of the transverse spatial coherence of the photon wavefunctions extending across the beam cross section. In the classical context, the interleaving approach was effectively used for polarization-sensitive beam splitting (*8*, *9*, *11*, *12*), yet it

requires nontrivial development for the application to multi-photon states.

We formulate and realize an application of the metasurface-based interferences for multi-photon quantum state measurement and reconstruction. We develop a metasurface incorporating a set of $M/2$ interleaved metagratings (see Part 3 in Ref. ([23])), each composed of nano-resonators with specially varying dimensions and orientation according to the principle of geometric-phase ([8]) to split specific elliptical polarization states ([7]), which would not be possible with conventional gratings (see Part 1 in Ref. ([23])). This performs quantum projections in a multi-photon Hilbert space to M imaging spots, each corresponding to a different elliptical polarization state [Fig. 1(A)], which is essential to minimize the error amplification in quantum state reconstruction ([24]). Then, by directly measuring all possible N-photon correlations from the M output beams, it becomes possible to reconstruct the initial N-photon density matrix providing full information on the multi-photon quantum entanglement. For example, in Fig. 1(B) we show a sketch of three gratings (top) which realize an optimal set of projective bases shown as vectors on the Poincaré sphere (middle) for $M = 6$.

The photon correlations between M output ports can be obtained with simple polarization-insensitive click single-photon detectors. The metasurface can be potentially combined with single-photon sensitive electron-multiplying CCD (EMCCD) cameras ([25], [26]) to determine the spatial correlations by processing multiple time-frame images of quantum states. We consider quantum states with a fixed photon number N, which is a widely-used approach in photon detection ([27]–[30]). The N-fold correlation data, stored in an array with N dimensions, are obtained by averaging the coincidence events over multiple time frames. For example, in Fig. 1(C) we sketch a case with $N = 2$ and $M = 6$. In each frame, two photons arrive at different combinations of spots. After summing up the coincidence events over multiple time frames, we obtain a correlation in two-dimensional space. Following the general measurement theory of Ref. ([30]), we establish that for an indistinguishable detection of N-photon polarization states (i.e. the

detectors cannot distinguish which is which of the N photons), the required number of output ports to perform the reconstruction scales linearly with the photon number as $M \geq N + 3$, see Fig. 1(B, bottom). For instance, with $M = 6$ up to $N = 3$ photon states can be measured.

The parallel realization of multi-photon interferences with a single metasuraface offers practical advantages for quantum state measurements. Conventional quantum state tomography (27) methods based on reconfigurable setups can require extra time and potentially suffer from errors associated with the movement of bulk optical components (27) or tuning of optical interference elements (31). Moreover, the conventionally-used sequential implementations of projective measurements present a fundamental limit for miniaturization, while being inherently sensitive to fluctuations or misalignment between different elements, especially for higher photon-number states. The emerging methods based on static transformations implemented with bulk optical components (19) or integrated waveguides (28–30) still require multiple stages of interferences. In contrast, our quantum metasurface provides an ultimately robust and compact solution, the speed of which is only limited by the detectors.

We fabricate silicon-on-glass metasurfaces with $M = 6$ and $M = 8$ using standard semiconductor fabrication technology (see Parts 4,7 in Ref. (23) for details). The experimentally determined polarization projective bases obtained through classical characterization are plotted on the Poincaré sphere in Fig. 2(A) for a metasurface with $M = 6$ that is used later for quantum experiments. The transfer matrix measurements confirm that the polarization projective bases are close to the optimal frame. The condition number, a measure of error amplification in the reconstruction (see Part 1 in Ref. (23)) is 2.08, close to the fundamental theoretical minimum of $\sqrt{3} \simeq 1.73$. The reconstruction is immune to fabrication imperfections, as their effect is fully taken into consideration by performing an experimental metasurface characterization with classical light after the fabrication (see Parts 6,10 in Ref. (23)).

First, we show that our metasurface enables accurate reconstruction of the quantum-

polarization state of single photons. A heralded photon source is used at a wavelength of 1570.6 nm based on spontaneous parametric down conversion (SPDC) in a nonlinear waveguide (see Parts 5,8,9,11 in Ref. (23) for details). The heralded single photons are initially linearly polarized. They are prepared in different polarization states by varying the angle of a quarter wave-plate (QWP), sent to the metasurface, and each diffracted photon beam is collected by a fiber-coupled interface to the single-photon detectors. By measuring the correlations with the master detector, we reconstruct the quantum-polarization state from the photon counts at the six ports. The results are shown in Fig. 2(B), where the curves are theoretical predictions and dots are experimental measurements. We observe that the measurement errors are dominated by the single-photon detection shot noise, which is proportional to the square root of the photon counts, as indicated by the error bars. We use the measured photon counts to reconstruct the input single-photon states by performing a maximum-likelihood estimation (27) and plot them on a Poincaré sphere in Fig. 2(C). The reconstructed states present a high average fidelity of 99.35% with respect to the prepared states.

Next, we realize two-photon interference, the setup of which is conceptually sketched in Fig. 3(A). The SPDC source generates a photon pair with horizontal (H) and vertical (V) polarizations, with their path length difference controllable by a delay-line (see Part 12 in Ref. (23) for details). We measure the effect of delay on the two-photon interference, analogous to the Hong-Ou-Mandel (HOM) experiment (32). In such a nontrivially generalized two-photon interference, we expect a dip or peak depending on the 2×2 transfer matrix $\mathbf{T_{ab}} \propto [\mathbf{u_a}, \mathbf{u_b}]^{\dagger}$ from the two-dimensional polarization state vector to a chosen pair of ports, where $\dagger$ denotes transpose conjugate, and $\mathbf{u}_a$, $\mathbf{u}_b$ are the projective basis of ports a and b, respectively. We note that $\mathbf{T_{ab}}$ corresponds to an effective Hermitian Hamiltonian resulting in a conventional HOM dip only if $\mathbf{u}_a$ and $\mathbf{u}_b$ are orthogonal, while otherwise a HOM peak can appear analogous to a lossy beam-splitter (22). Here we set the angle of the QWP at $\theta = 0°$, which means that the

photon pairs are in a state $\rho(\theta = 0°)$, where one photon is H- and another is V-polarized. As reflected in the Poincaré plot of Fig. 3(B, right), where the red arrows denote projective bases of the two ports ($\mathbf{u}_a$, $\mathbf{u}_b$) and blue arrows represent the polarization of the photon pairs – one photon in H- and the other in V-polarization, we see that the state vector $\mathbf{u_1}$ points to the opposite direction of $\mathbf{u_6}$. We find that in this case photons with cross-polarized entanglement in H-V basis will give rise to a dip in the interference pattern with the variation of path length difference, see Fig. 3(B, left). Such a behavior is directly caused by the coalescence nature of bosons. The situation is quite different if we measure such an interference between ports $a = 1$ and $b = 5$, since $\mathbf{u_1}$ and $\mathbf{u_5}$ are far from being orthogonal. This can be seen from the red arrows in the Poincaré sphere of Fig. 3(C, right), where the angle between the two vectors representing $\mathbf{u_1}$ and $\mathbf{u_5}$ is much smaller than π. For entangled photons with H and V polarization in a pair, interference under the transfer matrix $\mathbf{T_{15}}$ leads to a peak instead of a dip when varying the path difference in the delay-line. Indeed, in Fig. 3(C, left) we observe a peak, which is related to the anti-coalescence of bosons in transformations induced by non-Hermitian Hamiltonians, a nontrivial generalization of the HOM interference analogous to Ref. ([22]). For details of the theoretical predictions and experimental methods see Part 4 in Ref. ([23]).

As a following step, we measure all 15 two-fold nonlocal correlations between the $M = 6$ outputs from metasurface for a given input state where the time delay is fixed to zero. This provides us full information to accurately reconstruct the input two-photon density matrix. We use two single-photon detectors to map out all possible output combinations, while this could be potentially accomplished even simpler with an EMCCD camera. We show representative results for two different states $\rho(\theta = 0°)$ and $\rho(\theta = 37.5°)$ in Figs. 3(D,E) and 3(F,G), respectively. Note that $\rho(\theta = 0°)$ is a state where photon pairs have cross-polarized entanglement beyond the classical limit, yet it is not fully pure (see Part 4 in Ref. ([23])), providing a suitable test case for reconstruction of general mixed states. In Fig. 3(D) we show the measured two-

fold correlations for the input state $\rho(\theta = 0°)$, and the reconstructed density matrix is shown in Fig. 3(E). The fact that only the bunched four central elements are non-zero confirms cross-polarized property of our photon pairs in H-V basis. Moreover, the non-zero $|HVVH\rangle$ element implies the presence of two-photon entanglement. It is smaller compared to the diagonal element $|HVHV\rangle$, indicating that the polarization state is not fully pure. While $\rho(\theta = 0°)$ only has non-zero elements in the real part of the density matrix, we also show the measurement and reconstruction of $\rho(\theta = 37.5°)$ that contains nontrivial imaginary elements in Figs. 3(F,G). In both cases, we achieve a very good agreement between the predicted and reconstructed density matrices as evidenced by high fidelity exceeding 95%. The correlation counts are obtained by a Gaussian fitting to the correlation histogram to remove the background, which is less than 10% of the signal for all measurements shown in Fig. 3(F).

Our results illustrate the manifestation of multi-photon quantum interference on metasurfaces. We formulate a concept of parallel quantum state transformation with metasurfaces, enabling single- and multi-photon state measurements solely based on the interaction of light with sub-wavelength thin nanostructures and nonlocal correlation measurements without a requirement of photon-number-resolvable detectors. This presents the ultimate miniaturization and stability combined with high accuracy and robustness, as we demonstrate experimentally via reconstruction of one- and two-photon quantum-polarization states including the amplitude, phase, coherence and quantum entanglement. In general, our approach is particularly suitable for imaging-based measurements of multi-photon polarization states, where the metasurface can act as a quantum lens to transform the photons to a suitable format for the camera to recognize and retrieve more information. Furthermore, there is a potential to capture other degrees of freedom associated with spatially varying polarization states for the manipulation and measurement of high-dimensional quantum states of light, with applications including free-space communications and quantum imaging.

7

References

[1] N. F. Yu and F. Capasso, *Flat optics with designer metasurfaces*, Nat. Mater. **13**, 139–150 (2014).

[2] A. I. Kuznetsov, A. E. Miroshnichenko, M. L. Brongersma, Y. S. Kivshar, and B. Luk'yanchuk, *Optically resonant dielectric nanostructures*, Science **354**, 846–854 (2016).

[3] M. Decker, I. Staude, M. Falkner, J. Dominguez, D. N. Neshev, I. Brener, T. Pertsch, and Y. S. Kivshar, *High-Efficiency Dielectric Huygens' Surfaces*, Adv. Opt. Mater. **3**, 813–820 (2015).

[4] A. Arbabi, Y. Horie, M. Bagheri, and A. Faraon, *Dielectric metasurfaces for complete control of phase and polarization with subwavelength spatial resolution and high transmission*, Nat. Nanotechnol. **10**, 937–U190 (2015).

[5] S. Kruk, B. Hopkins, I. I. Kravchenko, A. Miroshnichenko, D. N. Neshev, and Y. S. Kivshar, *Invited Article: Broadband highly efficient dielectric metadevices for polarization control*, APL Photonics **1**, 030801–9 (2016).

[6] P. Genevet, F. Capasso, F. Aieta, M. Khorasaninejad, and R. Devlin, *Recent advances in planar optics: from plasmonic to dielectric metasurfaces*, Optica **4**, 139–152 (2017).

[7] J. P. B. Mueller, N. A. Rubin, R. C. Devlin, B. Groever, and F. Capasso, *Metasurface Polarization Optics: Independent Phase Control of Arbitrary Orthogonal States of Polarization*, Phys. Rev. Lett. **118**, 113901–5 (2017).

[8] Z. Bomzon, V. Kleiner, and E. Hasman, *Pancharatnam–Berry phase in space-variant polarization-state manipulations with subwavelength gratings*, Optics letters **26**, 1424–1426 (2001).

[9] A. Pors, M. G. Nielsen, and S. I. Bozhevolnyi, *Plasmonic metagratings for simultaneous determination of Stokes parameters*, Optica **2**, 716–723 (2015).

[10] J. P. B. Mueller, K. Leosson, and F. Capasso, *Ultracompact metasurface in-line polarimeter*, Optica **3**, 42–47 (2016).

[11] E. Maguid, I. Yulevich, D. Veksler, V. Kleiner, M. L. Brongersma, and E. Hasman, *Photonic spin-controlled multifunctional shared-aperture antenna array*, Science **352**, 1202–1206 (2016).

[12] F. Ding, A. Pors, Y. T. Chen, V. A. Zenin, and S. I. Bozhevolnyi, *Beam-Size-Invariant Spectropolarimeters Using Gap-Plasmon Metasurfaces*, ACS Photonics **4**, 943–949 (2017).

[13] R. C. Devlin, A. Ambrosio, N. A. Rubin, J. P. B. Mueller, and F. Capasso, *Arbitrary spin-to–orbital angular momentum conversion of light*, Science **358**, 896–901 (2017).

[14] P. K. Jha, X. J. Ni, C. H. Wu, Y. Wang, and X. Zhang, *Metasurface-Enabled Remote Quantum Interference*, Phys. Rev. Lett. **115**, 025501–5 (2015).

[15] T. Roger, S. Vezzoli, E. Bolduc, J. Valente, J. J. F. Heitz, J. Jeffers, C. Soci, J. Leach, C. Couteau, N. I. Zheludev, and D. Faccio, *Coherent perfect absorption in deeply sub-wavelength films in the single-photon regime*, Nat. Commun. **6**, 7031–5 (2015).

[16] A. Lyons, D. Oren, T. Roger, V. Savinov, J. Valente, S. Vezzoli, N. I. Zheludev, M. Segev, and D. Faccio, *Coherent metamaterial absorption of two-photon states with 40% efficiency*, arXiv 1709.03428 (2017).

[17] T. Stav, A. Faerman, E. Maguid, D. Oren, V. Kleiner, E. Hasman, and M. Segev, *Quantum metamaterials: entanglement of spin and orbital angular momentum of a single photon*, Science (2018).

[18] J. W. Silverstone, D. Bonneau, K. Ohira, N. Suzuki, H. Yoshida, N. Iizuka, M. Ezaki, C. M. Natarajan, M. G. Tanner, R. H. Hadfield, V. Zwiller, G. D. Marshall, J. G. Rarity, J. L. O'Brien, and M. G. Thompson, *On-chip quantum interference between silicon photon-pair sources*, Nature Photonics **8**, 104–108 (2014).

[19] O. Bayraktar, M. Swillo, C. Canalias, and G. Bjork, *Quantum-polarization state tomography*, Phys. Rev. A **94**, 020105–5 (2016).

[20] J. S. Fakonas, A. Mitskovets, and H. A. Atwater, *Path entanglement of surface plasmons*, New J. Phys. **17**, 023002–7 (2015).

[21] G. Di Martino, Y. Sonnefraud, M. S. Tame, S. Kena-Cohen, F. Dieleman, S. K. Ozdemir, M. S. Kim, and S. A. Maier, *Observation of Quantum Interference in the Plasmonic Hong-Ou-Mandel Effect*, Phys. Rev. Appl. **1**, 034004–6 (2014).

[22] B. Vest, M. C. Dheur, E. Devaux, A. Baron, E. Rousseau, J. P. Hugonin, J. J. Greffet, G. Messin, and F. Marquier, *Anti-coalescence of bosons on a lossy beam splitter*, Science **356**, 1373–1376 (2017).

[23] See supplementary materials.

[24] M. R. Foreman, A. Favaro, and A. Aiello, *Optimal Frames for Polarization State Reconstruction*, Phys. Rev. Lett. **115**, 263901–6 (2015).

[25] M. P. Edgar, D. S. Tasca, F. Izdebski, R. E. Warburton, J. Leach, M. Agnew, G. S. Buller, R. W. Boyd, and M. J. Padgett, *Imaging high-dimensional spatial entanglement with a camera*, Nat. Commun. **3**, 984–6 (2012).

[26] M. Reichert, H. Defienne, and J. W. Fleischer, *Massively Parallel Coincidence Counting of High-Dimensional Entangled States*, Sci. Rep. **8**, 7925–7 (2018).

[27] D. F. V. James, P. G. Kwiat, W. J. Munro, and A. G. White, *Measurement of qubits*, Phys. Rev. A **64**, 052312–15 (2001).

[28] J. G. Titchener, A. S. Solntsev, and A. A. Sukhorukov, *Two-photon tomography using on-chip quantum walks*, Opt. Lett. **41**, 4079–4082 (2016).

[29] D. Oren, M. Mutzafi, Y. C. Eldar, and M. Segev, *Quantum state tomography with a single measurement setup*, Optica **4**, 993–999 (2017).

[30] J. G. Titchener, M. Gräfe, R. Heilmann, A. S. Solntsev, A. Szameit, and A. A. Sukhorukov, *Scalable on-chip quantum state tomography*, npj Quant. Inform. **4**, 19 (2018).

[31] P. J. Shadbolt, M. R. Verde, A. Peruzzo, A. Politi, A. Laing, M. Lobino, J. C. Matthews, M. G. Thompson, and J. L. O'Brien, *Generating, manipulating and measuring entanglement and mixture with a reconfigurable photonic circuit*, Nature Photonics **6**, 45 (2012).

[32] C. K. Hong, Z. Y. Ou, and L. Mandel, *Measurement of subpicosecond time intervals between 2 photons by interference*, Phys. Rev. Lett. **59**, 2044–2046 (1987).

[33] E. Maguid, I. Yulevich, M. Yannai, V. Kleiner, M. L. Brongersma, and E. Hasman, *Multifunctional interleaved geometric-phase dielectric metasurfaces*, Light-Sci. Appl. **6**, e17027–7 (2017).

[34] L. E. Myers, R. C. Eckardt, M. M. Fejer, R. L. Byer, W. R. Bosenberg, and J. W. Pierce, *Quasi-phase-matched optical parametric oscillators in bulk periodically poled LiNbO$_3$*, J. Opt. Soc. Am. B **12**, 2102–2116 (1995).

[35] H. P. Chung, K. H. Huang, S. L. Yang, W. K. Chang, C. W. Wu, F. Setzpfandt, T. Pertsch, D. N. Neshev, and Y. H. Chen, *Adiabatic light transfer in titanium diffused lithium niobate waveguides*, Opt. Express **23**, 30641–30650 (2015).

[36] F. Lenzini, A. N. Poddubny, J. Titchener, P. Fisher, A. Boes, S. Kasture, B. Haylock, M. Villa, A. Mitchell, A. S. Solntsev, A. A. Sukhorukov, and M. Lobino, *Direct characterization of a nonlinear photonic circuit's wave function with laser light*, Light-Sci. Appl. **7**, 17143–5 (2018).

[37] W. K. Wootters, *Entanglement of formation of an arbitrary state of two qubits*, Phys. Rev. Lett. **80**, 2245–2248 (1998).

Acknowledgments

ences, which is a DOE Office of Science User Facility. **Author contributions:** K.W., D.N.N., and A.A.S. conceived and designed the research; K.W. and L.X. performed numerical modeling of metasurface design; S.S.K. and I.I.K. fabricated the dielectric metasurfaces; H.P.C. and Y.H.C. fabricated nonlinear waveguides; K.W., J.G.T., H.P.C., M.P., and A.S.S. performed optical experimental measurements and data analysis; A.A.S, D.N.N., and Y.S.K. supervised the work; K.W., A.A.S, D.N.N., and Y.S.K. prepared the manuscript and supplementary in contact with all authors. **Competing interests:** The authors declare no competing interests. **Data availability:** All data needed to evaluate the conclusions in this study are presented in the paper and/or in the supplementary materials (*23*).

Supplementary materials

Materials and Methods

Figs. S1 to S11

References (*33-37*)

Fig. 1. Concept of quantum state imaging via nanostructured flat optics. (A) Sketch of using a metasurface to image an input N-photon polarization state into an M-spot image. Top-right inset shows an SEM image of the fabricated all-dielectric metasurface. (C) Top – Sketch of three interleaved gratings for $M = 6$. Middle – the corresponding projective bases shown as vectors

on the Poincaré sphere. Bottom – minimum number of required spots to fully reconstruct the initial quantum state for different N, where optimal-frame choice of projective bases exists for M=6, 8, 12, 20, …. (C) An example of correlation measurement with N=2 and M=6, with several time-frame measurements combined into a two-dimensional correlation image.
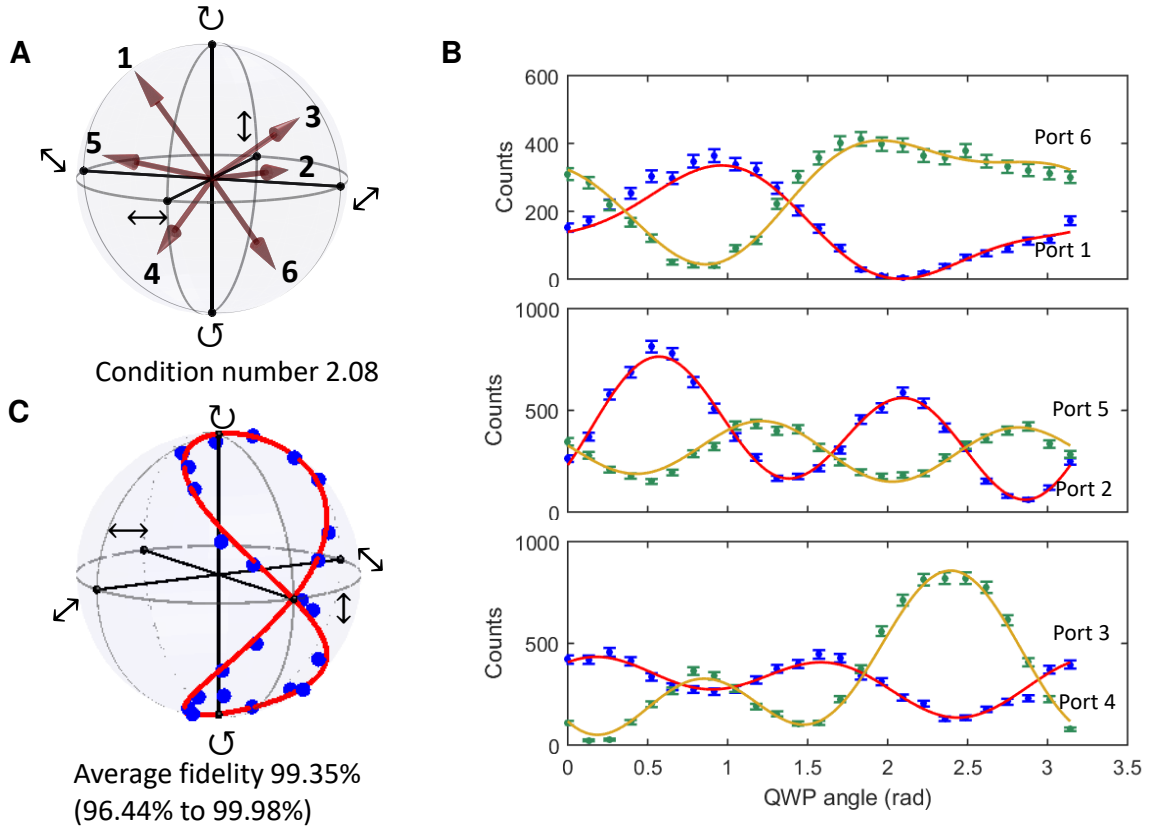
Fig. 2. Experimental measurement of heralded single-photon states with the metasurface. (A) Classically characterized projective bases of the metasurface for ports numbered 1 to 6. (B) Accumulated single-photon counts in each of M=6 output ports vs. the angle of a quarter-wave plate realizing a photon state transformation before the metasurface. Experimental data are shown with dots, with error bars indicating shot noise. Solid lines represent theoretical predictions based on classically measured metasurface transfer matrix. (C) Comparison between the prepared (solid line) and reconstructed (dots) states based on the measurements presented in (B), plotted on a Poincaré sphere.
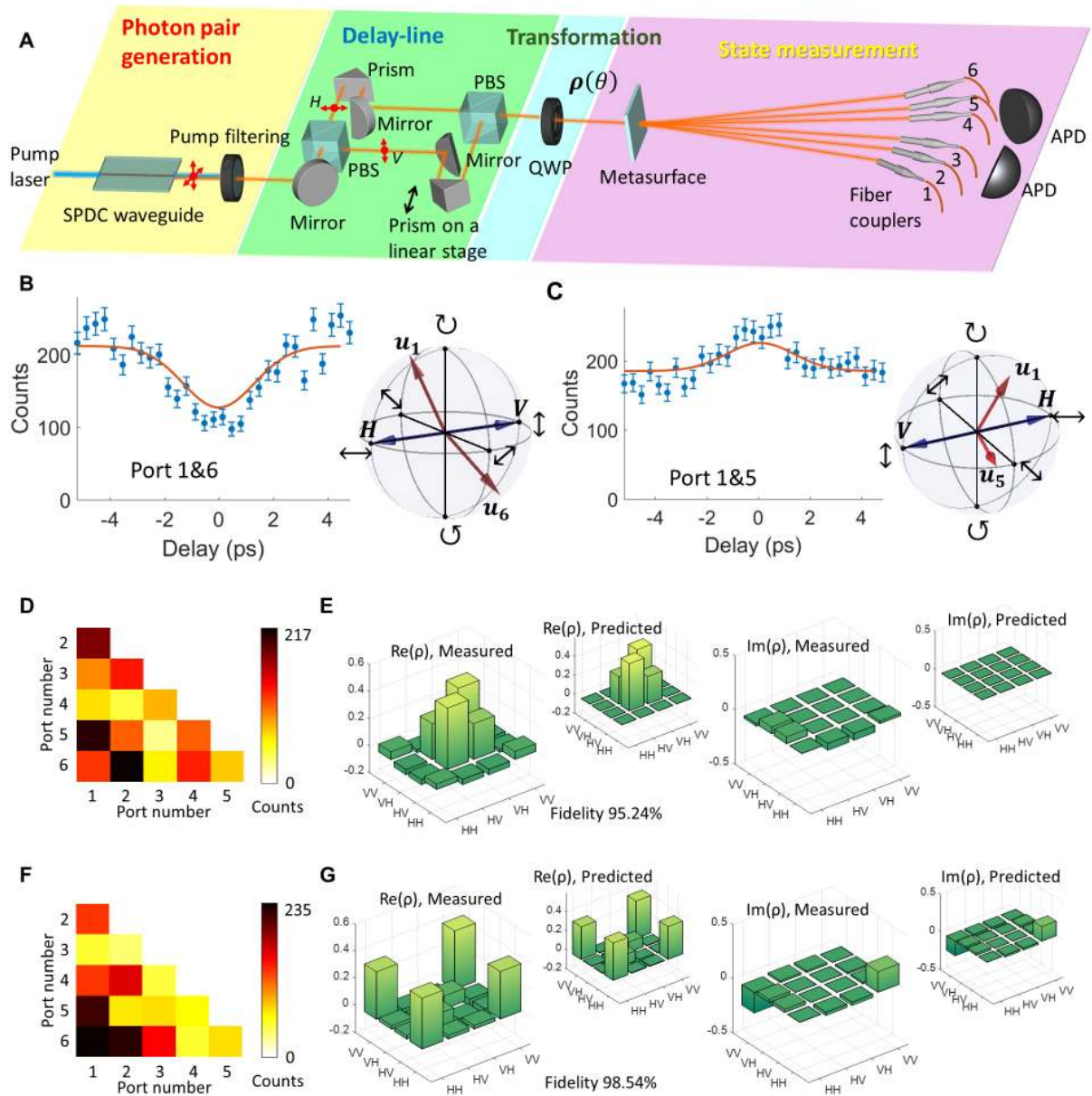
Fig. 3. Experimental two-photon interferences and state reconstruction with the metasurface. (A) Schematic setup including photon pair generation and pump filtering, a delay-line with polarizing beam splitters (PBS) to control the path difference between orthogonally polarized photons in a pair, state transformation with a quarter-wave plate (QWP), and state mea-

surement with the metasurface using avalanche photo-diodes (APDs). (B),(C) Quantum correlations between ports (B) 1 and 6 with close-to-orthogonal bases and (C) 1 and 5 with non-orthogonal bases, shown with dots and error bars indicating shot noise. Solid curves represent theoretical predications. Red arrows in the Poincaré spheres denote projective bases of different ports. Blue arrows indicate the polarization state of entangled photons, with one photon in H- and the other in V-polarization. (D),(F) Representative two-fold correlation measurements and (E),(G) the corresponding reconstructed density matrices ρ labeled 'Measured' alongside with the theoretically predicted states labeled 'Predicted' for QWP orientations (D),(E) $\theta = 0°$ and (F),(G) $\theta = 37.5°$.